

EDGE ARTICLE

View Article Online
View Journal | View Issue



Cite this: Chem. Sci., 2017, 8, 7689

A mitochondrial-targeted prodrug for NIR imaging guided and synergetic NIR photodynamic-chemo cancer therapy†

Hong-Wen Liu, (10) ‡ac Xiao-Xiao Hu, ‡a Ke Li, a Yongchao Liu, a Qiming Rong, a Longmin Zhu, a Lin Yuan, a Feng-Li Qu, b *b Xiao-Bing Zhang *b *a and Weihong Tan b a

Nontoxic prodrugs, especially activated by tumor microenvironment, are urgently required for reducing the side effects of cancer therapy. And combination of chemo-photodynamic therapy prodrugs show effectively synergetic therapeutic efficiency, however, this goal has not been achieved in a single molecule. In this work, we developed a mitochondrial-targeted prodrug PNPS for near infrared (NIR) fluorescence imaging guided and synergetic chemo-photodynamic precise cancer therapy for the first time. PNPS contains a NIR photosensitizer (NPS) and an anticancer drug 5'-deoxy-5-fluorouridine (5'-DFUR). These two parts are linked and caged through a bisboronate group, displaying no fluorescence and very low cytotoxicity. In the presence of H_2O_2 , the bisboronate group is broken, resulting in activation of NPS for NIR photodynamic therapy and activation of 5'-DFUR for chemotherapy. The activated NPS can also provide a NIR fluorescence signal for monitoring the release of activated drug. Taking advantage of the high H₂O₂ concentration in cancer cells, PNPS exhibits higher cytotoxicity to cancer cells than normal cells, resulting in lower side effects. In addition, based on its mitochondrial-targeted ability, PNPS exhibits enhanced chemotherapy efficiency compare to free 5'-DFUR. It also demonstrated a remarkably improved and synergistic chemo-photodynamic therapeutic effect for cancer cells. Moreover, PNPS exhibits excellent tumor microenvironment-activated performance when intravenously injected into tumor-bearing nude mice, as demonstrated by in vivo fluorescence imaging. Thus, PNPS is a promising prodrug for cancer therapy based on its tumor microenvironment-activated drug release, synergistic therapeutic effect and "turn-on" NIR imaging guide.

Received 8th August 2017 Accepted 11th September 2017

DOI: 10.1039/c7sc03454g

rsc.li/chemical-science

Introduction

Significant advances in cancer diagnosis and therapy have been made in the past years, but there still remain several barriers for improving effectiveness and avoiding severe side effects. ¹⁻⁵ This highlights the need to develop anticancer agents for effectively and selectively killing tumor cells without affecting normal tissues. Photodynamic therapy (PDT), driven by activating photosensitizers (PSs) to generate reactive oxygen species (ROS),

generally singlet oxygen for cancer cell killing, is considered to be a safe, minimally invasive treatment. 6,7 Highly selective photosensitizers are still desirable for accurately localizing and activatable prodrug to minimize side effects and realize more efficient therapeutic outcome. Recently, some activatable PSs have been developed for further minimizing the side effects of PDT.8,9 The design strategy is generally based on the concept that the prequenched fluorescence and inhibited phototoxicity of the PS which can be restored once a specific trigger is able to separate the quencher or energy acceptor from the vicinity of the PS.10,11 Moreover, the near infrared (NIR) PSs are desired for PDT, because NIR photons can deeply penetrate the skin and underlying tissue with low damage to the biological samples and minimal background interference.12-14 Therefore, it's very significant to develop activatable NIR PSs. On the other hand, chemotherapy is one of the most important modalities of cancer treatment. 5-Fluorouracil (5-FUra) has been used in the treatment of a variety of neoplastic diseases. 5'-Deoxy-5fluorouridine (5'-DFUR), a prodrug of 5-FUra, can be converted to 5-FUra by the thymidine phosphorylase, which is more abundant in tumors than in normal tissues except for the liver

^aMolecular Science and Biomedicine Laboratory, State Key Laboratory of Chemo/Biosensing and Chemometrics, College of Chemistry and Chemical Engineering, College of Life Sciences, Aptamer Engineering Center of Hunan Province, Hunan University, Changsha, 410082, P. R. China. E-mail: xbzhang@hnu. edu.cn

^bThe Key Laboratory of Life-Organic Analysis, College of Chemistry and Chemical Engineering, Qufu Normal University, Qufu, Shandong, 273165, P. R. China

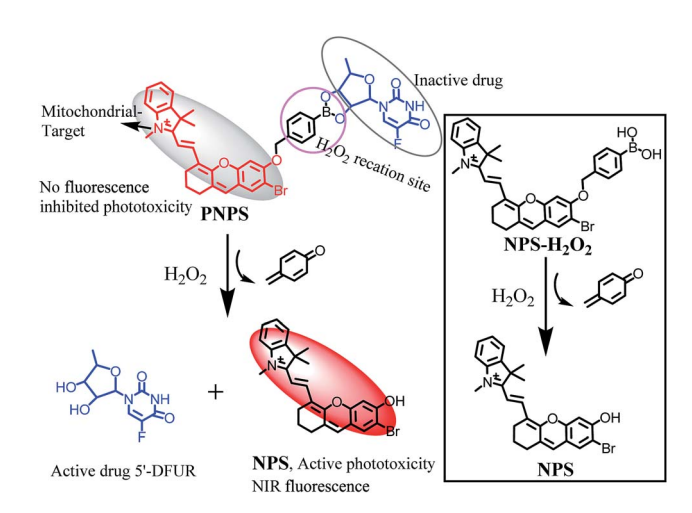
^{*}Key Laboratory of Environmentally Friendly Chemistry and Applications of Ministry of Education, College of Chemistry, XiangtanUniversity, Xiangtan 411105, P. R. China † Electronic supplementary information (ESI) available. See DOI: 10.1039/c7sc03454g

 $[\]ddagger$ These authors contributed equally to this work.

of humans. 15 The combination of PDT and chemotherapy with different therapeutic mechanisms has also been proved effective in improving the therapeutic efficiency,16 which has been achieved mainly via co-encapsulated an anticancer drug and a PS in nanocarriers. 17,18 In addition, since the extremely short half-life (<40 ns) and small radius of action (<20 nm) of singlet oxygen (1O2) in biological systems,19 direct delivering of PS to hypersensitive subcellular organelles will greatly enhance the PDT efficiency.20-22 Mitochondria are vital intracellular organelles that play valuable roles in energy production, ROS generation, cellular signalling and regulate apoptosis. Owing to the essential and fatal role of mitochondria, several mitochondrialtargeted anti-cancer drugs have been developed to expect optimal therapeutic efficiency.^{23,24} Many evidences also indicate that the damage of mitochondria is the main pathway for PDTtreated cell apoptosis.20 Thus, mitochondrion is the ideal subcellular target for cancer therapy.

The design of molecular fluorescent probe provides the strategy for developing theranostic prodrugs for targeted and image-guided combination cancer therapy.25 Fluorescent imaging can provide realtime informations about where, when, and how the prodrugs are delivered and activated in vivo.26 Generally, in such theranostic systems, masked anticancer drugs and imaging reagents are conjugated by tumor-sensitive linkers.27 Once in the tumor microenvironments, the tumorsensitive linkers can be broken by tumor over express species, such as low pH,28 high reactive oxygen species level (including H₂O₂),²⁹⁻³¹ high expressed enzymes,³²⁻³⁴ and high glutathione (GSH) concentration, 26,35-38 resulting in the release of the anticancer drugs and the activation of the imaging reagents. However, most of previous theranostic drugs do not realize combination of PDT and chemotherapy in a single molecule, which encouraged us to explore molecular theranostic probes with multi-function, including NIR PDT, chemotherapy, subcellular targeting and NIR fluorescence for real-time monitoring the therapeutic effect.

In this work, we developed a mitochondrial-targeted prodrug PNPS for NIR fluorescence imaging guided and synergetic chemo-photodynamic precise cancer therapy for the first time. PNPS is composed of two moieties and a specific recognition linker as shown in Scheme 1. The first moiety is a NIR fluorescent monitor NPS, of which its essential properties of NIR fluorescence and phototoxicity can be countered, yes reversed, by caging its hydroxyl group, act as a prodrug for PDT. Meanwhile, this NPS is preferably localized in mitochondria, due to its lipophilic quaternary ammonium salt structure.39 The second component is an anticancer drug 5'-DFUR. The former two parts are linked and caged through a H₂O₂-sensitive bisboronate group, displaying no flourescence signal and therapeutic effect. In the presence of H₂O₂, the bisboronate group is broken, resulting in releasing the free NPS for NIR PDT and free 5'-DFUR for chemotherapy. The activated NPS can also provide a NIR fluorescence signal for monitoring the release of the activated drugs. Taking advantages of the high H2O2 concentration in cancer cells, PNPS exhibited higher cytotoxicity to cancer cells than normal cells, resulting in lower side effects. In addition, based on its mitochondrial-targeted ability, PNPS



Scheme 1 Design of theranostic prodrug PNPS and proposed acti-

exhibited enhanced chemotherapy efficiency compare to free 5'-DFUR. Moreover, effective chemo-photodynamic combined therapy effects in cancer cells was observed. The in vitro and in vivo prodrug release was visualized by in situ generated NIR fluorescence. These favorable features microenvironment-activated ability, effective synergistic thertic effect and NIR fluorescence monitoring of the drug release make PNPS a promising prodrug.

Results and discussion

We first developed a novel NIR photosensitizer NPS, which shows the maximum excitation and emission wavelength at 680 nm and 710 nm, respectively. Since activatable photosensitizers share similar activation mechanisms with activatable fluorophores, the inherent fluorescence of NPS is prohibited accompany with inhibited phototoxicity, when the hydroxyl group of NPS is caged. Based on the molecular probe design strategy, we hypothesized to develop a subcellular targeted molecular theranostic prodrug with multi-function, such as fluorescence imaging, PDT, chemotherapy, and real-time monitoring of the therapeutic effect. H2O2 was chosen as the target for its high sensitivity and specificity toward the boronate moiety and intrinsic enhancement of H2O2 levels inside the tumor cell.40 It was easy to obtain prodrug NPS-H2O2 by attaching the H2O2 recognition group (benzoboric acid) to the hydroxyl group of NPS. And then, taking the advantage of the reaction between benzoboric acid and pinacol (5'-DFUR contains pinacol group), we obtained the final theranostic prodrug PNPS. The synthetic route for PNPS was depicted in Fig. S1.† And characterizations of all the new compounds are described in the ESI in detail.†

To verify that H₂O₂ was able to cleave the boronate moiety of prodrug PNPS and consequently activate the NIR fluorophore, a chemical transformation experiment of PNPS was performed in the presence of H₂O₂ under physiological conditions and monitored by UV-vis and fluorescence spectroscopy. In the UV-vis spectrum as shown in Fig. 1A, PNPS showed a strong

Edge Article

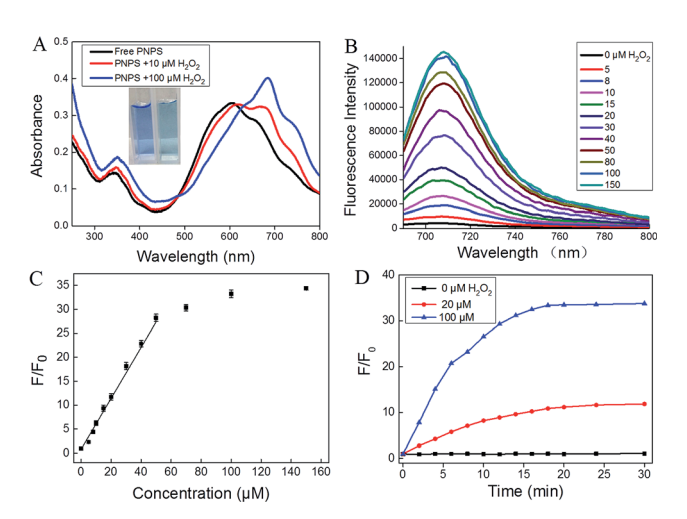


Fig. 1 (A) Absorption and (B) fluorescence emission spectra of PNPS (5 $\mu\text{M})$ with different concentration H_2O_2 in aqueous solution (PBS/DMSO =19:1, v/v, 10 mM, pH =7.4). Inset (A) photos of PNPS solution before (left) and after (right) addition of H_2O_2 . (C) Calibration curve of PNPS to H_2O_2 , the curve was plotted with the fluorescence intensity at 710 nm vs. H_2O_2 concentration. (D) A plot of fluorescence intensity at 710 nm of PNPS vs. the reaction time in the presence of varied concentrations of H_2O_2 . $\lambda_{ex}=680$ nm.

absorption peak at $\lambda_{max} = 600$ nm. The absorption peak showed a red shift after addition of 100 μM H₂O₂, accompanied by a distinct color change from blue to blue-green (Fig. 1A insert). As shown in Fig. 1B, PNPS exhibited weak fluorescence centered at 710 nm, and gradual addition of H₂O₂ up to 0-150 µM to a solution of PNPS induced the increase of fluorescence intensity. The fluorescence intensity at 710 nm increased by 34.3-fold upon reaction with 150 µM H₂O₂ for 30 min (Fig. 1C). Meanwhile, its intensity increased linearly with the concentration of H₂O₂ ranging from 5 to 40 μM (Fig. S2†). The catalytic efficiency of H2O2 toward the PNPS was assessed. Fluorescence kinetic curves of H₂O₂ at varied concentrations (0, 20, 100 μM) reacting with PNPS were depicted in Fig. 1D. As was shown, a higher concentration of H2O2 could induce faster cleavage reaction and therefore result in increased fluorescence intensity. The fluorescence signal of the reaction system could reach a plateau in about 20 min. Meanwhile, in the absence of H₂O₂, testing the generation of a false positive signal by spontaneous hydrolysis, gave no detectable signal increase, even over 12 h (Fig. S3†), demonstrating that PNPS was stable in the reaction system. These results demonstrated that after reaction with H₂O₂, PNPS was efficiently activated and the released NPS could provide a turn-on NIR fluorescence signal for drug release and therapeutic efficacy monitoring.

The selectivity of prodrug **PNPS** for H_2O_2 over other biologically relevant ROS species, metal ions, amino acids and proteins was evaluated. As shown in Fig. S4A,† no significant changes in fluorescence intensity were observed upon addition of the other ROS species, metal ions, amino acids and proteins to prodrug **PNPS**. The pH effect on the H_2O_2 -induced fluorescence changes of **PNPS** was also investigated. As shown in Fig. S4B,† **PNPS** remained stable and emitted a weak fluorescence within 4.0–9.0 pH range. After treatment by 25 μ M of

H₂O₂, the fluorescence at 710 nm was activated and reached saturation in the 7.4–8.0 pH range. The above results indicated that prodrug **PNPS** can be applied as a H₂O₂-activated theranostic prodrug under physiological pH condition with high selectivity.

To confirm the fluorescence response mechanism, the reaction products of **PNPS** with H_2O_2 were analyzed by HPLC and HRMS. As illustrated in Fig. S5,† pure **PNPS** showed a unique peak with retention time at about 5.36 min, and compound **NPS** exhibited a peak at about 6.25 min. After **PNPS** incubation with H_2O_2 for 30 min, a new peak at 6.25 min corresponding to compound **NPS** was clearly observed, and the peak corresponding to **PNPS** was sharply decreased. Moreover, in the ESI-HRMS (positive ion mode) spectrum of **PNPS** incubated with H_2O_2 for 30 min, the peaks of **NPS** and 5'-DFUR were found at m/z 464.1065 and 269.0462 respectively (Fig. S6†). These results demonstrated that the H_2O_2 cleaved recognition site, then **PNPS** was activated and free **NPS** and 5'-DFUR were released.

On the basis of the positive results showing H_2O_2 -activated release of active drug and concurrent fluorescence enhancement, **PNPS** was next tested in cultured cells. Cellular fluorescence imaging of **PNPS** were investigated in four different cell lines, HeLa, HepG2, HCT116 and HL7702 cells. HeLa, HepG2 and HCT116 cancer cells were pretreated with prodrug **PNPS** (5 μ M) for different time, then fluorescence imaging were carried out. The increased fluorescence intensity of HeLa, HepG2 and HCT116 cells indicated the efficient activation of theranostic **PNPS** by endogenous H_2O_2 in the tumor cells without any external inducer (Fig. 2A and S7–S9†). In addition, HeLa cells pretreated with exogenous H_2O_2 for 0.5 h and then incubated with **PNPS** for another 0.5 h, the fluorescence intensity dramatically increased. The cellular activation of **PNPS**

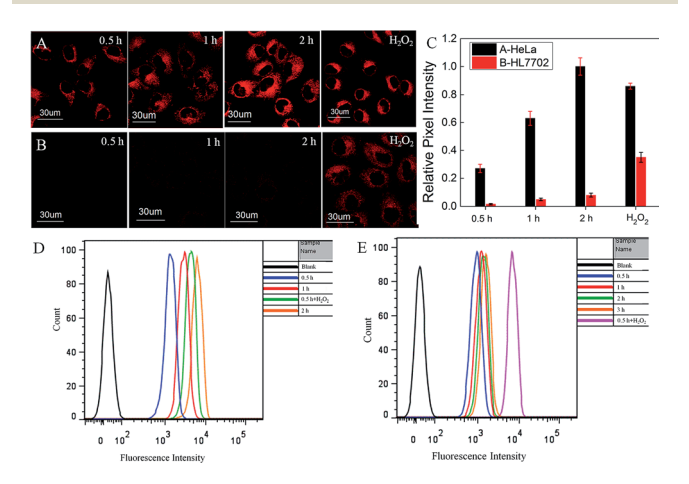


Fig. 2 Cellular fluorescence images of prodrug PNPS-treated HeLa (A) and HL7702 (B) cells. The cells were incubated with PNPS (5 μ M) for 0.5 h, 1 h and 2 h, respectively, or the cells were pretreated with H_2O_2 (100 μ M) for 0.5 h and then incubated with PNPS for another 0.5 h. (C) Relative pixel intensity (n = 3) from images (A and B). The pixel intensity from image (A) 2 h is defined as 1.0. Flow cytometric analysis of PNPS (5 μ M) fluorescence after incubated with HeLa (D) or HL7702 (E) cells for different time; or cells incubated with PNPS for 0.5 h and H_2O_2 (100 μ M) for another 0.5 h. $\lambda_{ex}=635$ nm, $\lambda_{em}=680-750$ nm.

were further confirmed by flow cytometry analysis (Fig. 2D). Similar phenomena were also observed in HepG2 cells (Fig. S8†), and the activation performance of PNPS in HepG2 after incubated for 2 h is 10% higher than that for HeLa cells calculated from the results of flow cytometry. These results indicated that the oxidation of boronate moiety of theranostic PNPS generated fluorescence enhancement, depending upon amount of intracellular H₂O₂, as depicted in Scheme 1. Normal HL-7702 cells were also incubated with prodrug PNPS for an examination of the effect of H₂O₂ on the bioactivity of PNPS. Very weak fluorescence signals were observed in HL-7702 cells by confocal microscopy after incubating with PNPS for 0.5 h, 1 h or 2 h (Fig. 2B). However, after pretreated with 100 μM H₂O₂ for 0.5 h, a strong fluorescent enhancement was observed in HL-7702 cells. The flow cytometry analysis results also confirmed that PNPS kept inactivated in HL-7702 cells (Fig. 2E). These results demonstrated that prodrug PNPS showed cancer cells-targeted activated ability.

Furthermore, mitochondrial localization of activated prodrug PNPS was investigated by colocalization experiments using a commercialized mitochondria fluorescent tracker, Mitotracker Green. As shown in Fig. 3 and S10,† the fluorescence signal that was ascribed to PNPS colocalized well with the Mitotracker (Pearson's correlation factor is 0.965, 0.943 and 0.958 for HeLa cells, HepG2 cells and HCT116 cells respectively), due to its lipophilic quaternary ammonium salt structure. Further experiments were carried out to demonstrate that most PNPS molecules will locate in mitochondria before reaction with cytoplasm H2O2, with the results showed in Fig S11.† This is mainly because the PNPS molecular can fast diffuse into cells and target mitochondria (within 10 min) before reaction with relatively low concentration cytoplasm H₂O₂. These results demonstrated the outstanding mitochondrial-targeting ability of PNPS, which may help improve the therapeutic effect.

The 1O_2 generation of **PNPS** in buffer solution in the present of H_2O_2 upon light irradiation was studied using 9, 10-diphenylanthracene (DPHA)⁴¹ and fluorescent probe MNAH⁴² as indicators. DPHA is a 1O_2 indicator, whose absorbance decreases upon interaction with 1O_2 . In the presence of H_2O_2 , when incubating DPHA with **PNPS** upon white light irradiation, the absorbance of DPHA decreased gradually (Fig. S12A†). Meanwhile, pretreated **PNPS** with H_2O_2 and then incubated with fluorescent probe MNAH upon white light irradiation, the fluorescence of MNAH increased gradually (Fig. S13A†). But in

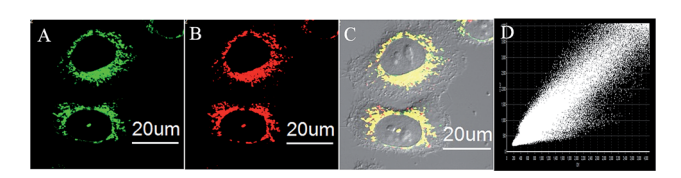


Fig. 3 Fluorescence images of co-localized experiment in HeLa cells. The cells were incubated with PNPS for 0.5 h and then incubated with MitoTracker Green for another 0.5 h. (A) MitoTracker Green (0.5 μ M, $\lambda_{\rm ex}=488$ nm, $\lambda_{\rm em}=500-550$ nm). (B) Prodrug PNPS (5 μ M, $\lambda_{\rm ex}=635$ nm, $\lambda_{\rm em}=680-750$ nm). (C) Overlay of (A) and (B). (D) Intensity correlation plot of stain, the Pearson's correlation factor is 0.965.

the absence of H₂O₂, the absorbance of DPHA or the fluorescence of MNAH showed limited changes (Fig. S12B and S13B†). And the compared results were shown in the Fig. 4A and Fig. 4B, obvious difference could be observed between those whether pretreated with H₂O₂. These results demonstrated that **PNPS** could efficiently generate ¹O₂ in buffer solution after activated by H₂O₂, indicated its activable phototoxicity. The ¹O₂ generation of **PNPS** in cells upon light irradiation was studied using 2',7'-dichlorofluorescin diacetate (DCF-DA) as a cell-permeable probe. DCF-DA is nonfluorescent but can be oxidized by ¹O₂ to yield highly fluorescent 2',7'-dichlorofluorescein (DCF). As shown in Fig. 4C, strong green fluorescence could only be observed when the cells were treated with **PNPS** for 2 h followed by light irradiation. The results confirmed the ¹O₂ generation by activated **PNPS** in live HeLa cells upon light irradiation.

We then investigated the ability of prodrug **PNPS** to selectively target cancer cells by measuring its cytotoxicity to HeLa, HepG2 and HL-7702 cells. MTS assays were used to study cytotoxicity of **PNPS**, **NPS-H**₂**O**₂ and 5'-DFUR under dark. After 3 h incubation, **NPS-H**₂**O**₂ and 5'-DFUR exhibited low cytotoxicity even at a high concentration of 15 μ M as more than 80% of the tested HeLa and HepG2 cells survived (Fig. 5). On the contrary, **PNPS** demonstrated much higher dark cytotoxicity with an IC₅₀ value of 16.6 μ M and 14.8 μ M for HeLa cells and HepG2 cells respectively (Fig. S14 and 15†). Taken together, these results illustrated that **PNPS** exhibited enhanced cytotoxicity over commercial 5'-DFUR. For **PNPS**, in addition to the high cytotoxicity under dark conditions, under white light

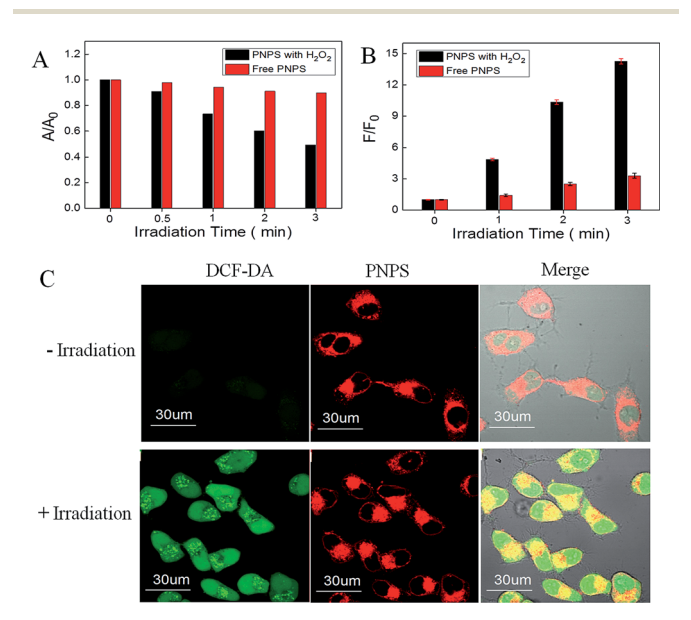


Fig. 4 (A) The change of DPHA absorbance at 373 nm in the presence of PNPS after different durations of white light irradiation. (B) The change of MNAH fluorescence intensity at 535 nm in the presence of PNPS after different durations of white light irradiation. The blank bar represents the reaction solution pretreated with $\rm H_2O_2$ for 0.5 h before light irradiation, the red bar represents without $\rm H_2O_2$ pretreatment. (C) Fluorescence imaging showing the $^1\rm O_2$ generation of PNPS (5 μ M) in HeLa cells after different treatments using (DCF-DA, 2 μ M) as indicator. The green channel is from DCF-DA (ex: 488 nm, em: 500–550 nm); the red channel is from PNPS ($\lambda_{\rm ex}=635$ nm, $\lambda_{\rm em}=680-750$ nm).

Edge Article



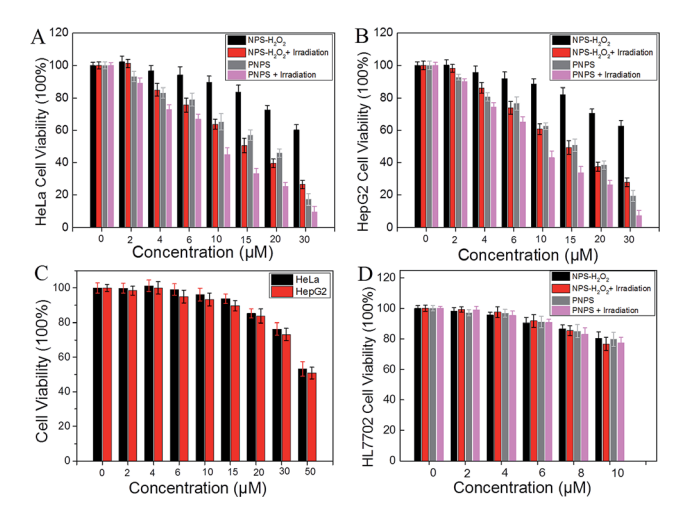


Fig. 5 Viability of (A) HeLa, (B) HepG2 and (D) HL7702 cells upon treatment with different concentrations of NPS-H2O2 or PNPS showed under white light irradiation or in dark. (C) Viability of HeLa (black bar) and HepG2 (red bar) cells upon treatment with different concentrations of 5'-DFUR

illumination, it could generate ¹O₂ and exhibited high phototoxicity to cancer cells. Notably, under white light illumination, the IC50 value of PNPS towards HeLa and HepG2 cells was 9.32 µM and 8.15 µM respectively (Fig. S14 and 15†), which was lower than that of PNPS without light irradiation (Fig. 5A and B). And compare to NPS-H2O2, PNPS showed enhanced cytotoxicity to cancer cells, due to its chemo-photodynamic combination therapy. However, both PNPS and NPS-H2O2 showed lower cytotoxicity even at a high concentration of 10 µM towards HL-7702 cells as more than 75% of the tested HL-7702 cells survived (Fig. 5D). As contrast, compound NPS exhibited high phototoxicity to HL-7702 cells (Fig. S16†), with IC₅₀ value of 8.50 μM (Fig. S17†). These results indicated that the prodrugs PNPS and NPS-H₂O₂ show low cytotoxicity to normal HL-7702 cells, which may mainly because that PNPS and NPS-H2O2 kept inactivated in HL-7702 cells. Collectively, these results demonstrated that the combination chemo-therapy and PDT provides higher anticancer effect compared to the single therapeutic approach alone.

The propidium iodide (PI) staining experiments were further carried out to demonstrate MTS results. PI, a cell impermeable

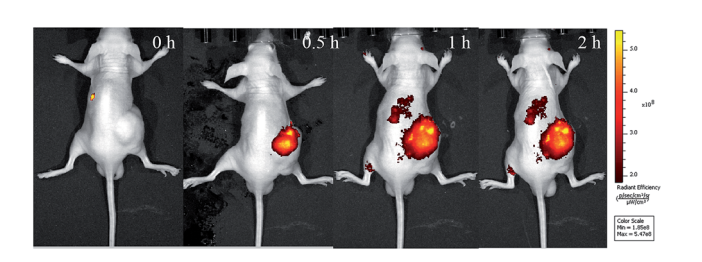


Fig. 6 In vivo imaging of HCT116 tumor-bearing mice at various time (0, 0.5, 1 h and 2 h) after orthotopic injection of the prodrug PNPS (0.288 mg kg⁻¹). 0 h means that the images was captured immediately after injection.

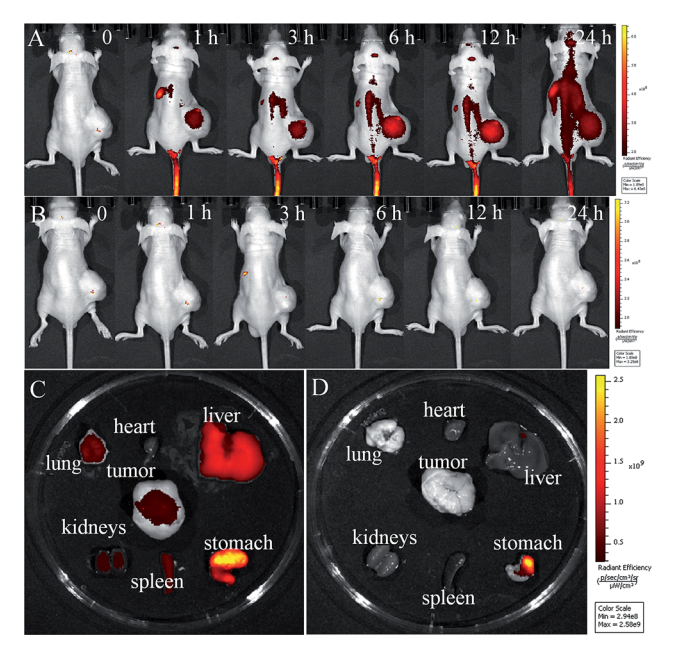


Fig. 7 In vivo imaging of HCT116 tumor-bearing mice at various times after intravenous injection of (A) prodrug PNPS (4.31 mg kg⁻¹) and (B) saline. Fluorescence images of the internal organs at 25 h post injection after anatomy for prodrug PNPS (C) and saline (D). 0 h means that the images was captured immediately after injection.

dye, only stains dead cells or late apoptotic cells with damaged membrane. As shown in Fig. S18,† PNPS-treated HeLa cells incubated under the dark was stained whereas nearly all the cells were stained after they were exposed to white light irradiation. Meanwhile, HL-7702 cells were incubated with PNPS much fewer cells were stained even after white light irradiation. However, when HL-7702 cells were first treated with H2O2 and follow with PNPS, most cells were stained after white light irradiation. Collectively, these results indicate that PNPS achieves lower side effects to normal cells.

Benefit from its NIR fluorescence, the activation of the prodrug PNPS in tumor-bearing mice could be investigated via in vivo fluorescence imaging. The nude mice bearing HCT116 xenografts were injected in the tumor site with the prodrug PNPS, and in vivo images were obtained at various times. As shown in Fig. 6, NIR fluorescence intensity representing the release of the activated drug, was clearly observed at 0.5 h after the injection of the PNPS, the NIR fluorescence then increased in time-dependent manner. These results indicated that theranostic prodrug PNPS could be effectively activated in the tumor and could be used for real-time fluorescence monitoring of the therapeutic effect in vivo.

We further investigated the activation and bio-distribution of prodrugs PNPS with HCT116 tumor-bearing mice, intravenously injected with PNPS and saline. As shown in Fig. 7A, the obvious fluorescence was seen in the tumor region after treated by prodrug PNPS for 1 h, indicative of the rapid distribution of PNPS via the blood circulation and the effective activation of PNPS in tumor. And a significant fluorescence enhancement was observed in tumor as time continued before 12 h post

injection due to the gradual prodrug activation, and it faded out as time further increased, owing to the excretion of the activated drug. In contrast, negligible signals were obtained in the saline-treated mice (Fig. 7B). And during the distribution process of 12 h, PNPS had the strongest fluorescence, representing the largest amount of released drug, in the tumor. These results indicated prominent tumor-targeting activation ability of PNPS. The tumor-targeting drug release along with fluorescence enhancement could be ascribed to the particularly high H₂O₂ concentration in cancer cells. Furthermore, in fluorescence images of the internal organs at 25 h post injection after anatomy, an obvious fluorescence was observed in the tumor, liver and stomach of mice treated by prodrug PNPS, and much weaker fluorescence were seen in lung, heart, kidney and spleen (Fig. 7C). Meanwhile, in the control experiments, no obvious fluorescence were observed in the tumor or other internal organs (Fig. 7D). The tumortargeting ability and the specific drug release in tumor make PNPS a promising prodrug to achieve high efficacy and reduced side effects.

Conclusions

In summary, by conjugating the anticancer drug 5'-DFUR and NIR photosensitizer (NPS) via a bisboronate bond, we developed a novel H₂O₂-responsive NIR theranostics prodrug **PNPS**. The phototoxicity and inherent NIR fluorescence of NPS and the cytotoxicity of the drug (5'-DFUR) are quenched by the covalent H₂O₂-responsive linker. PNPS can be effectively activated by the high concentration of H₂O₂ in cancer cells or in tumor as monitored by the turn-on NIR fluorescence. PNPS shows enhanced chemotherapy efficiency compare to free 5'-DFUR due to its mitochondrial-targeting ability. Furthermore, it shows remarkably improved and synergistic chemophotodynamic therapeutic effect for cancer cells. More importantly, PNPS exhibits higher cytotoxicity to cancer cells than that to normal HL-7702 cells, resulting in lower side effects. Therefore, the prodrug PNPS provides a promising platform for specific tumor-activatable drug delivery system, which can be easily monitored by cellular and in vivo NIR fluorescence imaging. This study also suggests that the molecular probe design strategy, which combines the key functions of targeting, release, imaging, and treatment within a single agent, may play an important role in cancer diagnosis and therapy.

Conflicts of interest

There are no conflicts to declare.

Acknowledgements

This work was supported by the National Natural Science Foundation of China (Grants 21325520, 21521063, 21327009, 21375076, J1210040), the science and technology project of Hunan Province (2016RS2009, 2016WK2002).

Notes and references

- 1 A. Umar, B. K. Dunn and P. Greenwald, *Nat. Rev. Cancer*, 2012, **12**, 835–848.
- 2 P. E. Goss and A. F. Chambers, *Nat. Rev. Cancer*, 2010, 10, 871–877.
- 3 X. Li, J. Kim, J. Yoon and X. Chen, Adv. Mater., 2017, 29, 1606857.
- 4 H. Ju, Sci. China: Chem., 2015, 58, 438.
- 5 W. Pan, H. Yang, T. Zhang, Y. Li, N. Li and B. Tang, *Anal. Chem.*, 2013, **85**, 6930–6935.
- 6 J. P. Celli, B. Q. Spring, I. Rizvi, C. L. Evans, K. S. Samkoe, S. Verma, B. W. Pogue and T. Hasan, *Chem. Rev.*, 2010, 110, 2795.
- 7 A. P. Castano, P. Mroz and M. R. Hamblin, *Nat. Rev. Cancer*, 2006, 6, 535–545.
- 8 X. S. Li, S. Kolemen, J. Yoon and E. U. Akkaya, *Adv. Funct. Mater.*, 2017, 27, 1604053.
- 9 S. Kolemen, M. Isik, G. M. Kim, D. Kim, H. Geng, M. Buyuktemiz, T. Karatas, X. F. Zhang, Y. Dede, J. Yoon and E. U. Akkaya, *Angew. Chem., Int. Ed.*, 2015, 54, 5340–5344.
- 10 J. F. Lovell, T. W. B. Liu, J. Chen and G. Zheng, *Chem. Rev.*, 2010, **110**, 2839–2857.
- 11 R. Musiol, M. Serda and J. Polanski, Curr. Pharm. Des., 2011, 17, 3548–3559.
- 12 Z. Guo, S. Park, J. Yoon and I. Shin, *Chem. Soc. Rev.*, 2014, 43, 16–29.
- 13 X. Chen, D. Lee, S. Yu, G. Kim, S. Lee, Y. Cho, H. Jeong, K. T. Nam and J. Yoon, *Biomaterials*, 2017, 122, 130–140.
- 14 N. Li, Z. Yu, W. Pan, Y. Han, T. Zhang and B. Tang, *Adv. Funct. Mater.*, 2013, 23, 2255–2262.
- 15 H. Eda, K. Fujimoto, S.-i. Watanabe, M. Ura, A. Hino, Y. Tanaka, K. Wada and H. Ishitsuka, *Cancer Chemother. Pharmacol.*, 1993, 32, 333–338.
- 16 M. Olivo, R. Bhuvaneswari, S. S. Lucky, N. Dendukuri and P. Soo-Ping Thong, *Pharmaceuticals*, 2010, 3, 1507–1529.
- 17 W. Zhang, J. Shen, H. Su, G. Mu, J.-H. Sun, C.-P. Tan, X.-J. Liang, L.-N. Ji and Z.-W. Mao, *ACS Appl. Mater. Interfaces*, 2016, **8**, 13332–13340.
- 18 Y. Zhang, F. Huang, C. Ren, L. Yang, J. Liu, Z. Cheng, L. Chu and J. Liu, ACS Appl. Mater. Interfaces, 2017, 9, 13016–13028.
- 19 P. R. Ogilby, Chem. Soc. Rev., 2010, 39, 3181-3209.
- 20 R. Hilf, J. Bioenerg. Biomembr., 2007, 39, 85-89.
- 21 L. Rajendran, H. J. Knolker and K. Simons, *Nat. Rev. Drug Discovery*, 2010, **9**, 29–42.
- 22 Z. Yu, W. Pan, N. Li and B. Tang, *Chem. Sci.*, 2016, 7, 4237–4244.
- 23 S. Fulda, L. Galluzzi and G. Kroemer, *Nat. Rev. Drug Discovery*, 2010, **9**, 447–464.
- 24 Z. Yu, Q. Sun, W. Pan, N. Li and B. Tang, *ACS Nano*, 2015, **9**, 11064–11074.
- 25 C.-J. Zhang, Q. Hu, G. Feng, R. Zhang, Y. Yuan, X. Lu and B. Liu, *Chem. Sci.*, 2015, **6**, 4580–4586.
- 26 M. Z. Ye, X. H. Wang, J. B. Tang, Z. Q. Guo, Y. Q. Shen, H. Tian and W. H. Zhu, *Chem. Sci.*, 2016, 7, 4958–4965.

Edge Article

- 27 M. Gao, F. Yu, C. Lv, J. Choo and L. Chen, *Chem. Soc. Rev.*, 2017, 46, 2237–2271.
- 28 J.-Z. Du, X.-J. Du, C.-Q. Mao and J. Wang, *J. Am. Chem. Soc.*, 2011, 133, 17560–17563.
- 29 Y. Y. Yuan, C. J. Zhang, S. D. Xu and B. Liu, *Chem. Sci.*, 2016, 7, 1862–1866.
- 30 E.-J. Kim, S. Bhuniya, H. Lee, H. M. Kim, C. Cheong, S. Maiti, K. S. Hong and J. S. Kim, *J. Am. Chem. Soc.*, 2014, 136, 13888– 13894.
- 31 R. Kumar, J. Han, H.-J. Lim, W. X. Ren, J.-Y. Lim, J.-H. Kim and J. S. Kim, *J. Am. Chem. Soc.*, 2014, **136**, 17836–17843.
- 32 Y. Ichikawa, M. Kamiya, F. Obata, M. Miura, T. Terai, T. Komatsu, T. Ueno, K. Hanaoka, T. Nagano and Y. Urano, *Angew. Chem., Int. Ed.*, 2014, 53, 6772–6775.
- 33 Y. Y. Yuan, C. J. Zhang, M. Gao, R. Y. Zhang, B. Z. Tang and B. Liu, *Angew. Chem., Int. Ed.*, 2015, 54, 1780–1786.
- 34 G. Zheng, J. Chen, K. Stefflova, M. Jarvi, H. Li and B. C. Wilson, *Proc. Natl. Acad. Sci. U. S. A.*, 2007, **104**, 8989–8994.

- 35 F. P. Kong, Z. Y. Liang, D. R. Luan, X. J. Liu, K. H. Xu and B. Tang, *Anal. Chem.*, 2016, **88**, 6450–6456.
- 36 X. Wu, X. Sun, Z. Guo, J. Tang, Y. Shen, T. D. James, H. Tian and W. Zhu, *J. Am. Chem. Soc.*, 2014, **136**, 3579–3588.
- 37 S. Bhuniya, S. Maiti, E. J. Kim, H. Lee, J. L. Sessler, K. S. Hong and J. S. Kim, *Angew. Chem., Int. Ed.*, 2014, 53, 4469–4474.
- 38 S. Santra, C. Kaittanis, O. J. Santiesteban and J. M. Perez, *J. Am. Chem. Soc.*, 2011, **133**, 16680–16688.
- 39 L. Yuan, W. Lin, S. Zhao, W. Gao, B. Chen, L. He and S. Zhu, J. Am. Chem. Soc., 2012, 134, 13510–13523.
- 40 E. W. Miller and C. J. Chang, *Curr. Opin. Chem. Biol.*, 2007, 11, 620-625.
- 41 Y. Yuan, C.-J. Zhang, S. Xu and B. Liu, *Chem. Sci.*, 2016, 7, 1862–1866.
- 42 H.-W. Liu, S. Xu, P. Wang, X.-X. Hu, J. Zhang, L. Yuan, X.-B. Zhang and W. Tan, *Chem. Commun.*, 2016, **52**, 12330–12333.